ELSEVIER

Chemical Engineering Science 63 (2008) 1997–2005

Chemical Engineering Science

www.elsevier.com/locate/ces

Adsorption behaviors of organic vapors using mesoporous silica particles made by evaporation induced self-assembly method

Chin-Te Hung, Hsunling Bai*

Institute of Environmental Engineering, National Chiao Tung University, 75 Po-Ai Street, Hsinchu 300, Taiwan

Received 30 September 2007; received in revised form 17 December 2007; accepted 2 January 2008
Available online 9 January 2008

Abstract

Spherical mesoporous silica materials with controllable surface area and uniform pore size were synthesized via evaporation induced self-assembly (EISA) method in this study. Both well-ordered and less-ordered mesoporous silica particle (MSP) adsorbents were made via adjusting the surfactant/silica precursor molar ratio. And the relationships between the physical characteristics of MSP adsorbents and the acetone adsorption behaviors were examined for the first time. The results indicated that an increase in the specific surface area results in an increase in the acetone adsorption capacity. But if a further increase in the surface area causes a less structured adsorbent then the acetone adsorption capacity could become less even though the specific surface area is of the highest value of 1337 m^2/g. The acetone adsorption capacity of well-ordered MSP adsorbent is more than twice of that of the commercial ZSM-5 zeolite adsorbent due to its relatively higher surface area and uniform pores. The well-ordered structure of MSP also leads to higher acetone adsorption efficiency and a sharper breakthrough curve due to fast pore diffusion.

Keywords: Adsorption; Volatile organic compounds (VOCs); Mesoporous silica particles; Evaporation induced self-assembly; ZSM-5 zeolite

1. Introduction

Volatile organic compounds (VOCs) are major air pollutants in industrial processes and environmental activities which must be controlled under stringent environmental regulations in many countries. There are commercialized VOCs control technologies such as combustion, adsorption, absorption, biofiltration, and catalytic oxidation. And adsorption is one of the most widely employed methods in practical industrial operation because of the easy operation and low cost with efficient recovery of most VOCs (Ruhl, 1993). Porous adsorbents such as activated carbon (AC) and zeolite are commercially available for VOCs treatment. And new mesoporous silica materials such as MCM-41 have been widely studied on adsorption of VOCs (Zhao et al., 2001).

The most important characteristics of porous adsorbents are their surface properties such as porous structure, pore size distribution, wall thickness, specific surface area, and hydrophilic–hydrophobic properties. However, efforts on comparison of VOCs adsorbents or catalysts have often been based on adsorbents of complicated pore structure with pore scales that may range from micro- to macro-sizes. Serrano et al. (2007) have reported the adsorption properties of different zeolites and indicated that the affinity to adsorbates resulted from the fact that elemental framework plays an important role on the adsorption. However, information on the relationship between VOCs adsorption and the pore structure of adsorbents is still limited. This leads to difficulty in systematically analyzing the adsorption behaviors during either adsorption or catalysis processes.

In recent years, controlling the physical property of porous adsorbent becomes easier due to the progress in nanomaterial preparation technologies. The MCM-41 firstly manufactured by mobile (Beck et al., 1992) and mesoporous silica particles (MSP) was then modified from the MCM-41 materials by Lu et al. (1999). The MSP was produced by an evaporation induced self-assembly (EISA) method and it combines the simplicity of sol–gel process and aerosol-assisted process with the efficiency of surfactant self-assembly The principle of EISA route for producing MSP is that the evaporation of solvent in

* Corresponding author. Tel.: +886 3 5731868; fax: +886 3 5725958.
E-mail address: hlbai@mail.nctu.edu.tw (H. Bai).

0009-2509/$ - see front matter © 2008 Elsevier Ltd. All rights reserved.
doi:10.1016/j.ces.2008.01.002

precursors during aerosol process causes multi-phased assembly of surfactant micelle, which resulted in the inward meso-structure of silica droplets in a synthesized time of only several seconds. Thus rapid synthesis of mesoporous structured materials is the major advantage of EISA as compared to the hydrothermal method for producing MCM-41.

This study intends to synthesize MSP via EISA method and investigate its adsorption performance on the removal of acetone, which is one of the most common VOCs emitted from semiconductor and opto-electronic industries. A systematic analysis on the effects of specific surface area and pore structure of MSP adsorbent on the acetone adsorption behaviors is performed.

2. Experiments

2.1. Synthesis of MSP

Fig. 1 shows the experimental setup for the preparation of MSP adsorbents via EISA method. Cetyltrimethyl ammonium bromide (CTAB) was used as the structure-directing template and tetraethyl orthosilicate (TEOS) was used as the silica precursor. The molar gel composition of the synthesized mixture was TEOS: x CTAB: 10 ethanol: 40 H_2O: 0.008 HCl (x varies from 0.06 to 0.26). The reagents were mixed and nebulized by an ultrasonic atomizer and carried by a high-pressure, clean, and dry air flow. Then the reagent flow was passed through a high-temperature tubular reactor with two heating zones. The total flow rate was set at 2.0 LSTPmin^{-1}.

The heating length was 50 cm and the inner tube diameter was 1.27 cm for each heating zone. The first and second heating zones of the reactor were controlled at temperatures of 150 and 550 °C, respectively. The first heating zone was used for self-organization of the particles via solvent evaporation. The second heating zone provides temperature for the calcination, inorganic condensation, and densification of the particles. After the heating processes, MSP were collected on a high-efficiency filter maintained at a temperature of 150 °C to avoid water condensation. Finally, the collected MSP were further calcined at 550 °C for 4 h to eliminate the organic structure-directing template (Lu et al., 1999; Lin et al., 2005).

2.2. Characterization of MSP

The morphology and structure of MSP adsorbents were characterized by using transmission electron microscopy (TEM, Hitachi H-7100, Japan) and X-ray diffraction (XRD, Rigaku D/MAX-B, Japan, using Cu Kα radiation n source at 1.54 Å). The Brunauer–Emmett–Teller (BET) specific surface area of the materials was measured by N_2 adsorption–desorption isotherms at 77 K using a surface area and porosimetric instrument (Micromeritics ASAP 2020, USA). The synthesized samples were out-gassed at 350 °C for 4 h under high vacuum before the surface area measurement. The specific pore volume, average pore diameter, and pore size distribution were obtained from the nitrogen adsorption and desorption isotherms by Barrett–Joyner–Halenda (BJH) theory.

2.3. Acetone adsorption test

Acetone was selected as the target adsorbate in this study. A thermo-gravimetric analyzer (TGA, Netzsch TG209 F1, Germany) was used to measure the equilibrium adsorption capacity of acetone. MSP adsorbents were loaded on the TGA sample holder and purged with nitrogen gas at temperature of 200 °C for 1 h before acetone adsorption test. The mass change of MSP adsorbents during acetone adsorption was then measured under isothermal condition of 25 °C. The inlet acetone concentration was 15 000 ppmv; it is the saturated concentration at 25 °C as obtained by passing the N_2 gas stream into two impingers containing liquid acetone. The flow rate was 65 cm^3/min during each adsorption experiment. The equilibrium adsorption capacity of acetone was determined until negligible weight change (less than 0.01% difference) was observed.

A packed column test was also performed for obtaining the breakthrough curve and for simulating the practical adsorption process. The adsorbent of $\sim$ 200 mg was packed inside an

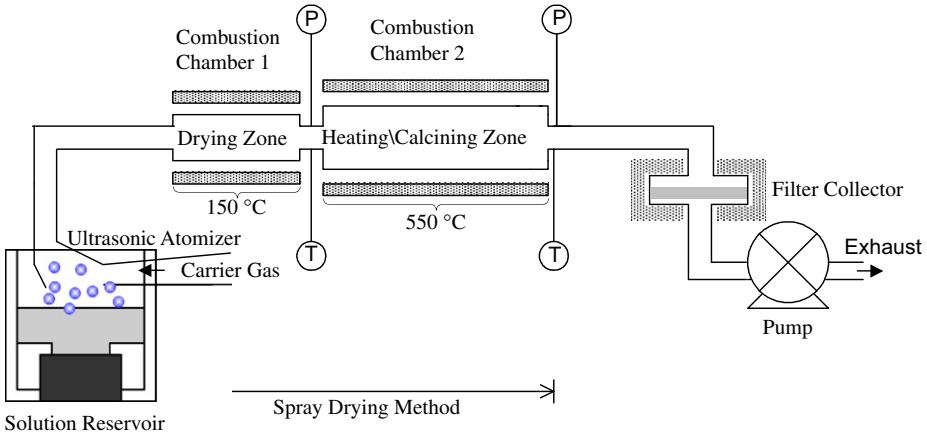

Fig. 1. Experimental setup for synthesizing mesoporous silica particle (MSP) adsorbents via evaporation induced self-assembly (EISA) method.

adsorption column of 1 cm i.d. Under a typical test, the acetone inlet concentration was 1000 ppmv as diluted with clean air. But for the adsorption isotherm tests, the acetone inlet concentration ranged from 100 to 1500 ppmv. The packed column tests were performed at 25 °C with a total system flow rate of 500 cm^3/ min. The inlet and outlet acetone concentrations were measured by GC-FID (SRI 8610C, USA).

3. Results and discussion

3.1. Characterization of MSP adsorbents

The synthesized samples are denoted as S-*X*, where *X* corresponds to the precursor molar ratio of CTAB surfactant to TEOS silica source (Surf/Si). For example, S06 and S26 indicated that the adsorbent samples were prepared under Surf/Si molar ratios of 0.06 and 0.26, respectively.

The TEM images of MSP adsorbents produced at various Surf/Si molar ratios are shown in Fig. 2. The surface texture of S06 illustrated in Fig. 2(a) shows rough surface structure with irregular pores. The formation of less-ordered mesopores at low surfactant concentration may be because that CTAB surfactant concentration could not thoroughly overtake the critical micelle concentration (CMC) during the evaporation process (Baccile et al., 2003).

The TEM images of S12 and S18 samples shown in Figs. 2(b) and (c), respectively, indicated that these two adsorbent samples have better-ordered pore structures. In the Surf/Si molar ratio region of 0.12–0.18, the CMC of forming rod shape micelles can be achieved during alcohol and water evaporation

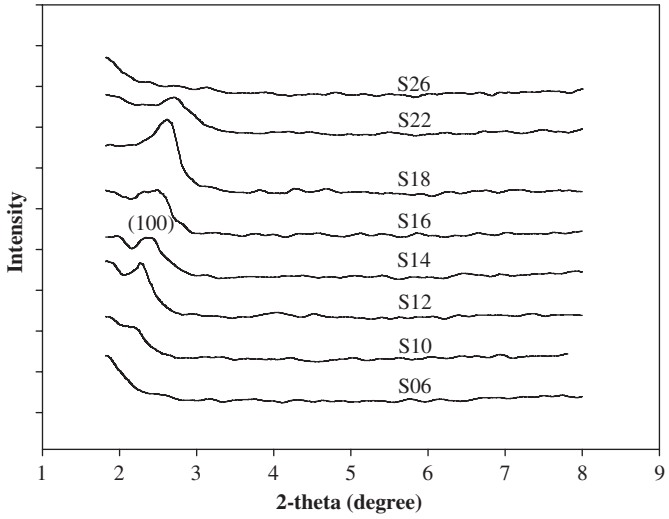

Fig. 3. X-ray diffraction patterns of MSP adsorbents.

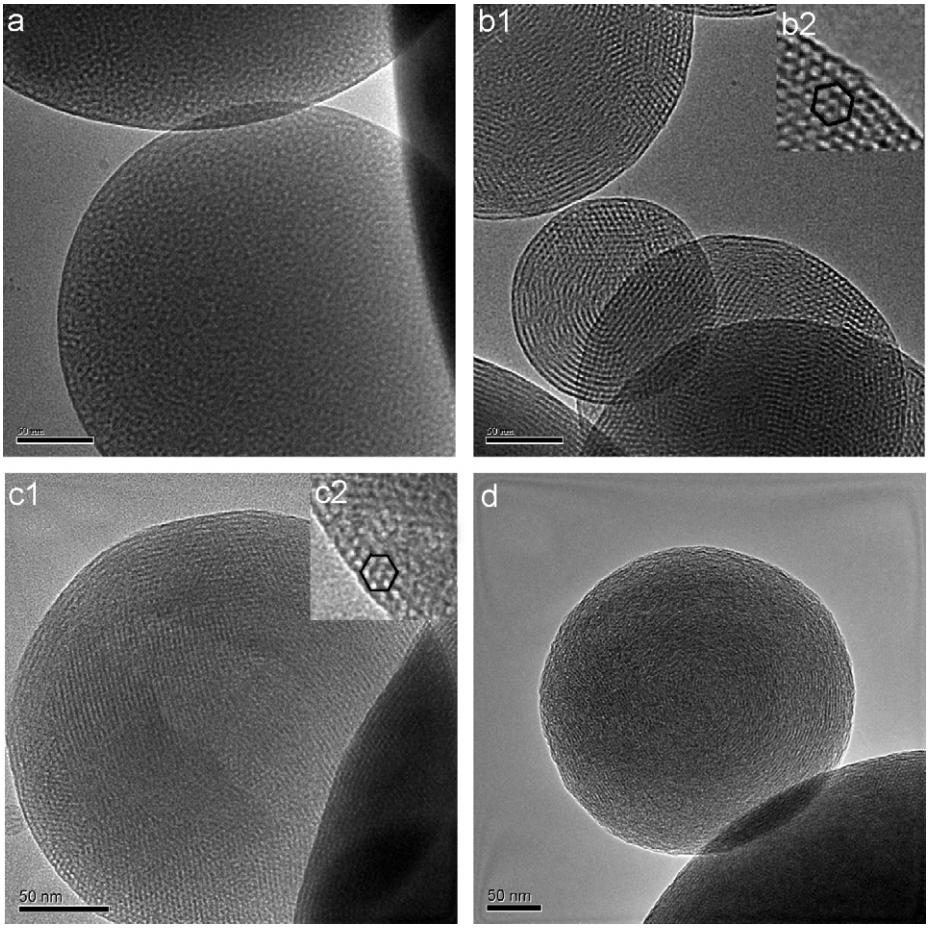

Fig. 2. TEM images of MSP adsorbents: (a) S06, (b) S12, (c) S18, (d) S22. The scale bar in the images is 50 nm.

Table 1
Physical properties of porous silica adsorbent particles characterized by XRD and BET analyses

Sample name	Surf/Si molar ratio	V_p[a] (cm^3/g)	S_{BET}[b] (m^2/g)	d_{BJH}[c] (nm)	d_{100}[d] (nm)	Unit cell a[e] (nm)	T_w[f] (nm)
S06	0.06	0.355	424	2.7	–	–	–
S10	0.10	0.606	754	2.5	4.1	4.7	2.1
S12	0.12	0.682	856	2.5	3.9	4.6	2.0
S14	0.14	0.794	1006	2.5	3.7	4.4	1.9
S16	0.16	0.750	1073	2.4	3.6	4.1	1.7
S18	0.18	0.895	1153	2.4	3.4	3.9	1.5
S22	0.22	0.935	1337	2.5	3.3	3.8	1.3
S26	0.26	0.637	1252	–	–	–	–

[a]Pore volume.
[b]BET surface area.
[c]Pore diameter calculated by BJH theory.
[d]d-spacing between (1 0 0) planes.
[e]Hexagonal unit cell (Eq. (2)).
[f]Pore wall thickness (Eq. (1)).

so that ordered 2D-hexagonal structure can be formed. And the hexagonal structure of the samples can be clearly observed in the enlarged TEM images of Figs. 2(b-2) and (c-2). The mesoporous order is constructed of either arranged hexagonal spots (i.e., tubular pores perpendicular to the particle surface) or tubular pores parallel to the particle surface. This observation is similar to that in the literature (Bore et al., 2003). The MSP adsorbents made by EISA process are spherical shape particles with 2D-hexagonal structure, while the MCM-41 materials made by hydrothermal method are usually in irregular shapes with 1D-hexagonal structure. And by comparing with 1D-hexagonal MCM-41 material of oriented pore structure, the domain of hexagonally ordered tubular pores was smaller than that of MCM-41 materials. The 2D-hexagonal structure may be due to the bending of rod micelle of surfactant in order to fit into the spherical shape of particles.

Fig. 2(d) illustrates the TEM image of S22 sample. One can see that there is apparent disorder in the surface structure of mesoporous particles. The formation of less-ordered pore structure may be due to the partial collapse of rod micelle structure during the surfactant removal. Another reason to explain less-ordered pore structure is the formation of new shape micelles such as vesicles and reverse micelles that decrease the uniformity during self-assembly of micelles (Baccile et al., 2003; Bore et al., 2003).

The mesoporous structures of the samples were confirmed by XRD patterns as shown in Fig. 3. The (1 0 0) diffraction peaks located at about $2\theta = 2.3$–$2.7°$ are more clearly observed for samples prepared under Surf/Si molar ratios of around 0.12–0.18. This reveals the evidence of more-ordered mesoporous structure. One can also see from Fig. 3 that the XRD peaks tend to be shifted to larger angles as the Surf/Si molar ratio is increased, which leads to the decreases of d-spacing values, i.e., center-to-center pore distance as listed in Table 1, and will be discuss in the detail in the next section.

The intensities of diffraction peak for S12–S18 samples are higher than that of S22 sample, which means that the uniformity of mesopores and the order of structure for Surf/Si = 0.12–0.18 are better. The presence of broadening and reduction in the intensity of diffraction peak for S22 sample further confirms the collapse of some pores and thus leads to the less-ordered mesoporous structure. Both a further increase of the Surf/Si molar ratio beyond 0.22 and a decrease of Surf/Si molar ratio below 0.10 result in the flattening of XRD peaks at $2\theta = 2.3$–$2.7°$. This is consistent with the TEM images shown in Fig. 2.

3.2. Surface area analysis

The nitrogen adsorption and desorption isotherms of MSP adsorbents as prepared under various Surf/Si molar ratios are shown in Fig. 4. The nitrogen adsorption/desorption isotherms for S06–S22 samples exhibit a type IV isotherm based on IUPAC classifications. This is typical for mesoporous solid particles with a slight hysteresis and indicates narrow pore size distributions of the samples. Samples prepared under Surf/Si molar ratios of 0.06–0.22 reveal a rapid increase in the adsorption quantity at a relative pressure range of 0.2–0.3, which is the evidence of capillary condensation of nitrogen molecules in the primary mesopores. The S26 sample displays a different adsorption/desorption isotherm from other samples. Its isotherm curve appears to be a type I isotherm based on the IUPAC classification, which is typical of microporous structure.

Fig. 5 shows the BJH pore size distributions of S06–S26 samples. The BJH pore size distributions of all samples except S26 display narrow pore size distributions with mode diameter of around 2.4–2.5 nm. And the peak of pore size distribution for S18 sample is higher than the other samples This indicates that S18 sample has the most uniform mesoporous structure. On the other hand, the BJH pore size distribution of S26 is shifted to the micropore region of less than 2 nm and thus it could not be detected in this study. The result is consistent with the nitrogen adsorption/desorption isotherms as shown previously in Fig. 4 that S26 has a type I isotherm curve of microporous structure.

The values of BJH pore diameter (d_{BJH}) for all samples are listed in Table 1. As S06–S22 samples were prepared by the same surfactant they do not show significant difference and range from 2.4 to 2.7 nm. The specific surface area (S_{BET}),

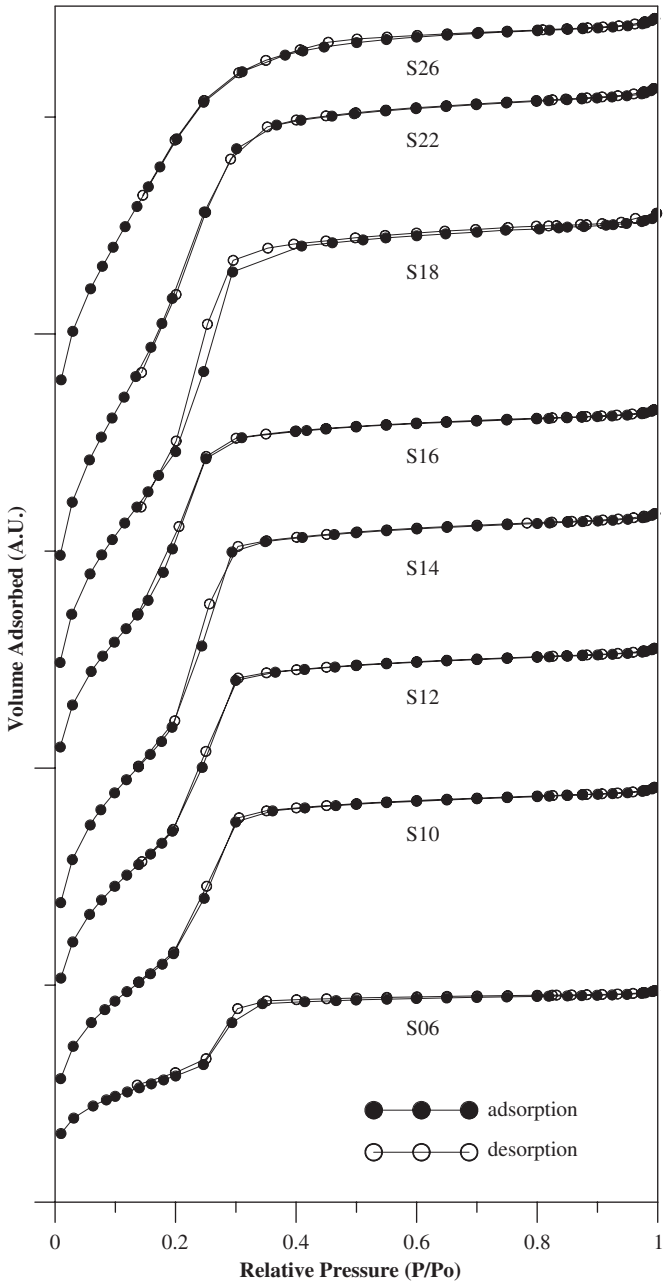

Fig. 4. Nitrogen adsorption/desorption isotherms of MSP adsorbents.

specific pore volume (V_p), and wall thickness of all the samples (T_w) are listed in Table 1. The specific surface area for S06–S26 samples ranges from 424 to 1337 m^2/g, and it increases with increasing the Surf/Si molar ratio up to 0.22. Both the maximum surface area and pore volume are achieved by sample made from Surf/Si molar ratio of 0.22.

The pore wall thickness (T_w) was calculated by taking the difference between the hexagonal unit cell parameter (a) and the BJH pore diameter (d_{BJH}) with the assumption that mesopores in all samples are presented in a perfect hexagonal structure:

$$T_w = a - d_{BJH}. \quad (1)$$

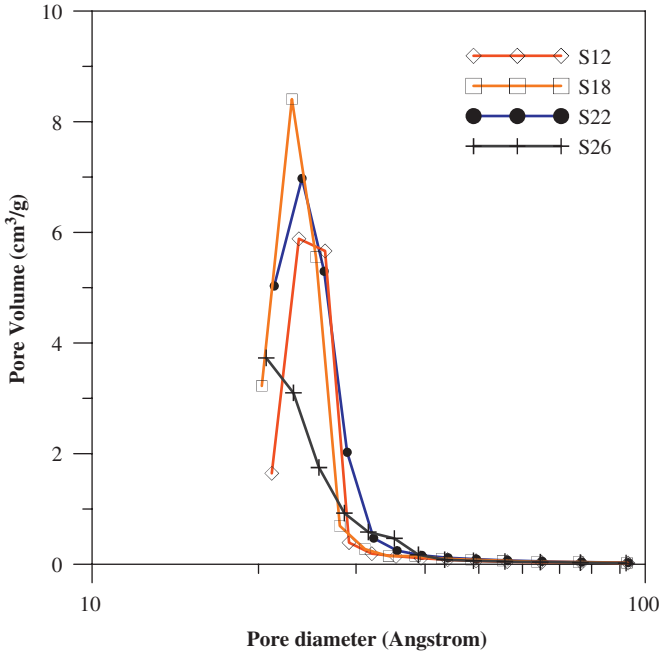

Fig. 5. BJH pore diameter distributions of MSP adsorbents.

The hexagonal unit cell parameter (a) is related to d-spacing (d_{100}) (Kruk et al., 1997) by

$$a = 2d_{100}/\sqrt{3}. \quad (2)$$

The calculated results are listed in Table 1 and they reveal that the pore wall thickness decreases from 2.1 to 1.3 nm as the Surf/Si molar ratio increases form 0.06 to 0.26.

From Table 1 it is known that the BET surface area and the wall thickness of the samples can be controlled by adjusting the Surf/Si molar ratio. The Surf/Si molar ratio, the BET surface area, and the wall thickness were found to be in a good linear relationship for the Surf/Si molar ratio range of 0.12–0.18. Thus, for well-ordered MSP adsorbents the surface area and the wall thickness of the pore could be easily controlled by adjusting the Surf/Si molar ratio within the range of 0.12–0.18.

3.3. Optimal Surf/Si molar ratio

The molar ratio of Surf/Si is the most important parameter that controls the physical properties of MSP adsorbents. The concentration of surfactant affects the formed micelles and determines the shape and order of mesopores in the particles (Baccile et al., 2003; Bore et al., 2003; Lu et al., 1999). The well-ordered hexagonal structure of MSP was obtained using optimal Surf/Si molar ratios between 0.12 and 0.18. Similar results were obtained by Baccile et al. (2003), who reported the optimal molar ratios ranging from 0.15 to 0.25. The difference in the optimal molar ratio is mainly caused by operating conditions and the amount of precursor solvent.

The evaporation time of mixture from atomized droplets depends markedly on the system flow rate and the initial surfactant concentration. Appropriate evaporation time can enhance

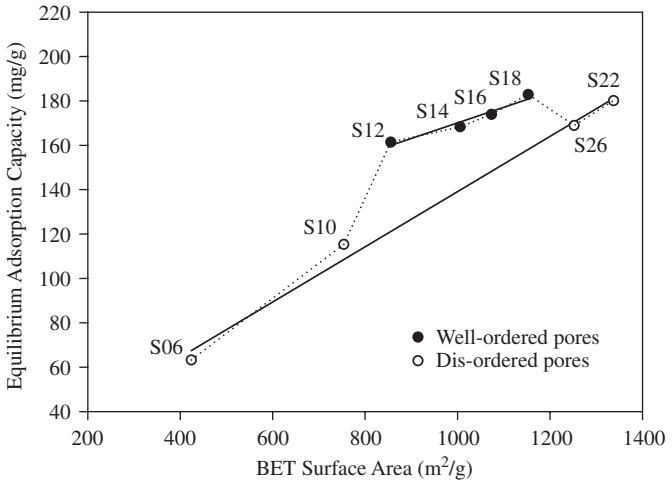

Fig. 6. Equilibrium acetone adsorption capacity of MSP adsorbents from TGA analyses at an acetone inlet concentration of 15 000 ppmv. Both well-ordered and less-ordered MSP show linear relationship between acetone adsorption capacity and specific surface area. But the well-ordered MSP has a significant increase in the adsorption capacity.

the formation of micelles with a well self-assembled hexagonal structure. The system flow rate in the report of Baccile et al. (2003) was 1.5 times higher as compared to this study. It led to the decrease of evaporation\drying time.

In addition, the amount of ethanol concentration in the report of Baccile et al. (2003) is triple as compared to that used in this study. The concentration of alcohols in the sol–gel mixture is critically important for the formation of self-organization of micelles into periodic meso-structures. It was reported (Li et al., 2006) that the CMC of the surfactant increased with the increase of ethanol concentration in the ethanol/water/CTAB mixtures, thus resulting in the gradual decrease of the micelle size. This is because a small amount of co-solvent (ethanol) in the water/CTAB mixtures can promote the surfactant solubility and enhance the micelle formation.

3.4. Acetone adsorption and mass transfer zone

Fig. 6 displays the equilibrium acetone adsorption capacity of the MSP adsorbents measured by TGA as a function of specific surface area. It is interesting to note that the adsorption capacity of MSP adsorbents can be divided into two distinct groups by linear regression. The upper group includes S12, S14, S16, and S18 samples, which are the well-ordered mesoporous structural MSP adsorbents. The other group includes S06, S10, S22, and S26 samples, which are the less-ordered porous or worm-like structural MSP adsorbents. As observed from the result, well-ordered mesoporous structural MSP adsorbents lead to better acetone adsorption capacities as compared to less-ordered ones. But both groups show linear increases of the acetone adsorption capacity with the specific surface area. This is reasonable since all mesoporous silica samples have similar values of pore diameter.

The maximum adsorption capacity is 183 mg/g for S18 sample (Surf/Si molar ratio of 0.18). This is in accord to its higher

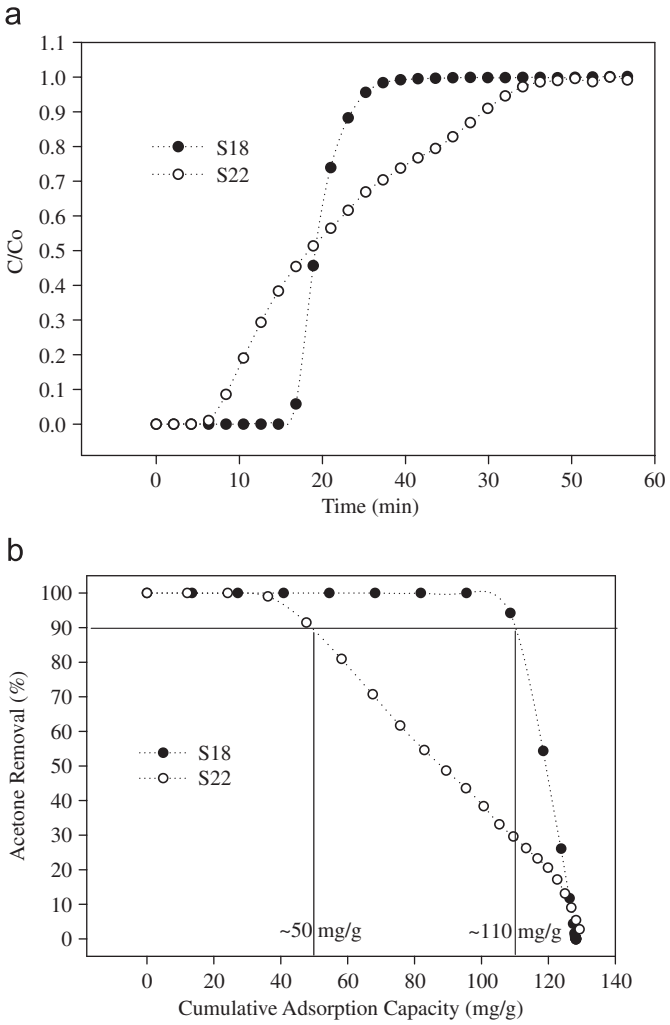

Fig. 7. (a). Breakthrough curves for S18 (well ordered) and S22 (less ordered) MSP adsorbents from packed column tests at an acetone inlet concentration of 1000 ppmv. (b). Acetone removals as a function of cumulative adsorption capacity for S18 (well ordered) and S22 (less ordered) MSP adsorbents from packed column tests. The break point was set at 90% acetone removal.

specific surface area. However, a further increase of the specific surface area for S22 and S26 samples does not lead to a further increase of the acetone adsorption capacity as compared to the S18 sample. This might be due to the limitation of less uniformity in the pore structure that restrained the internal diffusion of acetone adsorbate in the pores. Thus, the pore structure of adsorbent is also a key factor for its adsorption capacity. From the above results, one can know that the highest adsorption capacity did not occur on S22 sample with the highest specific surface area. The highest adsorption capacity appears for S18 sample which has a lower surface area but more uniform pore structure.

To further clarify the effect of porous structure, packed column adsorption tests for S18 and S22 adsorbents were performed. Fig. 7(a) shows the breakthrough curves of S18 and S22 adsorbents. As can be seen from the breakthrough curves, the S18 adsorbent provides a sharper breakthrough curve (thus a thin mass transfer zone) as well as a higher adsorption capacity

than those of S22 adsorbent. This may be due to differences in the effective internal diffusion arising from differences in pore tortuosity or connectivity. The S22 adsorbent which has a less-organized pore structure should have longer diffusion time in the pores thus resulting in a broader breakthrough curve (thus a thick mass transfer zone).

Fig. 7(b) shows the acetone removal as a function of cumulative adsorption capacity. For practical application, the adsorbent in an adsorber should be replaced at the break point. And by setting a typical break point of 90% acetone removal for VOCs abatement of semiconductor and opto-electronic industries, it is observed that although both samples have similar adsorption capacity of $\sim 130\,mg/g$ at exhaustion, the advantage of thin mass transfer zone for S18 adsorbent results in a better adsorption capacity at the break point. The cumulative acetone adsorption capacity at 90% acetone removal for S18 sample is around 110 mg/g, which is more than twice that of S22 sample, 50 mg/g.

In addition, acetone adsorption isotherms are examined by the packed column tests. Experimental data were fitted to the well-known isotherm models of Langmuir (1916, 1918) and Freundlich (1906):

$$\text{Langmuir:} \quad \frac{C_e}{q_e} = \frac{1}{q_0 K_L} + \frac{1}{q_0} C_e, \tag{3}$$

$$\text{Freundlich:} \quad \log q_e \log K_F + \frac{1}{n_F} \log C_e, \tag{4}$$

Where C_e (ppmv) and q_e (mg/g) are the gas phase concentration and solid phase adsorption quantity of acetone at equilibrium, respectively; K_L is the Langmuir isotherm constant; q_0 (mg/g) is the single layer acetone adsorption capacity; K_F is the Freundlich constant; and n_F is the heterogeneity factor.

Fig. 8(a) illustrates the Langmuir adsorption isotherm of S18 and S22 MSP adsorbents and Fig. 8(b) shows the Freundlich adsorption isotherm of them for adsorbing 100–1500 ppmv of acetone vapors. The Langmuir and Freundlich adsorption isotherm parameters for the adsorption of acetone vapors onto S18 and S22 MSP adsorbents are listed in Table 2. The fitted results of both Langmuir and Freundlich isotherms showed good correlation with R^2 values > 0.96. This indicates that the two adsorption isotherm models are both reasonable for describing acetone adsorption behaviors at acetone concentrations of 100–1500 ppmv. The values of $n_F > 1$ in Freundlich model as seen in Table 2 reflected favorable adsorption of acetone vapors onto S18 and S22 MSP adsorbents. On the basis of the Langmuir analysis, the single layer acetone adsorption capacities q_0 are calculated to be 175.4 and 161.3 mg/g for S18 and S22 MSP adsorbents, respectively, as listed in Table 2.

3.5. Comparison with ZSM-5 zeolite adsorbent

The ZSM-5 zeolite adsorbent is one of the most popular commercial adsorbents for semiconductor and opto-electronic industries on the VOCs adsorption (Chang et al., 2003). Thus, if the MSP can have a better adsorption capacity then it will have high potential to replace the zeolite for commercial application.

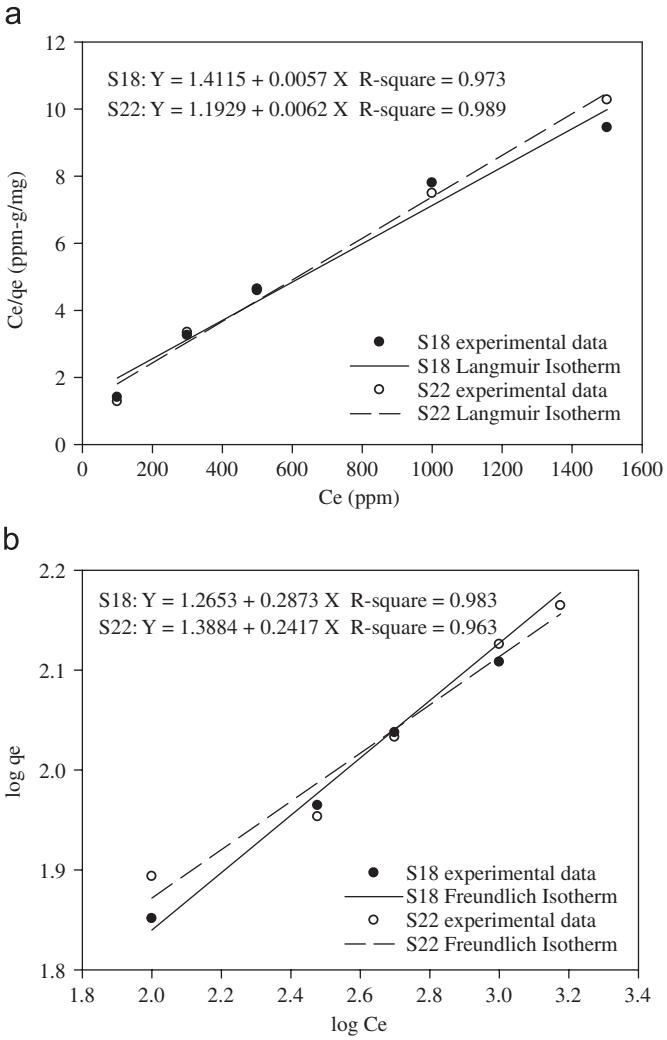

Fig. 8. (a). Langmuir adsorption isotherm for S18 and S22 MSP adsorbents. (b). Freundlich adsorption isotherm for S18 and S22 MSP adsorbents.

Fig. 8 shows the comparison of equilibrium acetone adsorption capacity as well as cumulative adsorption capacity at 90% removal between commercial ZSM-5 zeolite (CBV8014, Zeolyst, $SiO_2/Al_2O_3 = 80$) and S18 MSP adsorbents.

The ZSM-5 zeolite was expected to have higher affinity to acetone molecules due to their relatively higher polarities as compared to the pure siliceous MSP adsorbent; thus it should lead to a better adsorption capacity than hydrophobic MSP adsorbent. This was observed in the authors' previous studies (Lin et al., 2005; Lin and Bai, 2006). The surface area of MSP made by Lin and Bai (2006), $872\,m^2/g$, was about twice that of the commercial ZSM-5 zeolite, $420\,m^2/g$. But their acetone adsorption capacity was about the same as or even less than that of the ZSM-5 zeolite.

In this study, an optimization of the process leads to much higher surface area of S18 sample ($1153\,m^2/g$) as well as a better-ordered pore structure that provides more adsorption sites and fast adsorption rate. Thus, the resulting acetone adsorption capacity of S18 adsorbent becomes more than that of ZSM-5 zeolite as observed in Fig. 9. The equilibrium acetone

Table 2
Summary of the Langmuir and Freundlich isotherm constants

Isotherm	Adsorbent	Parameters		*R*-square
		q_0 (mg/g)	K_L (1/ppm)	
Langmuir	S18	175.44	0.0050	0.973
	S22	161.29	0.0052	0.989
		K_F	n_F	
Freundlich	S18	18.42	3.48	0.983
	S22	24.46	4.14	0.963

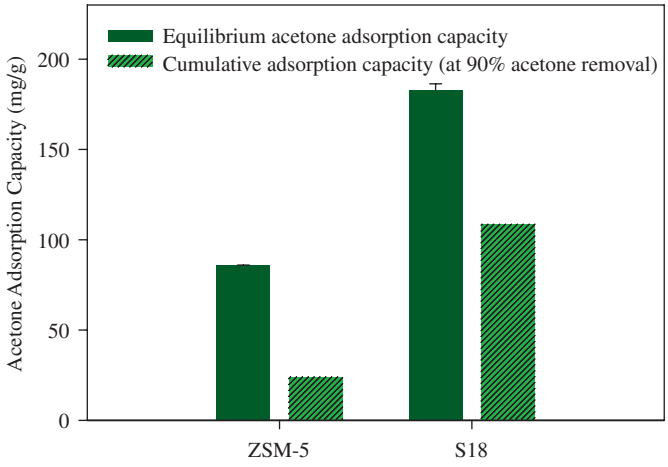

Fig. 9. Comparison of the equilibrium acetone adsorption capacity and cumulative adsorption capacity at 90% acetone removal between S18 MSP adsorbent and commercial ZSM-5 zeolite.

adsorption capacity of S18 adsorbent is 183 mg/g, which is more than twice that of the ZSM-5 zeolite adsorbent, 86 mg/g. While for 90% removal of acetone, the cumulative acetone adsorption capacity of MSP is around 110 mg/g, which is much better than that of ZSM-5 zeolite, 24 mg/g. This provides a high advantage for practical adsorption application using S18 adsorbent since it can be operated at a high acetone removal efficiency with much less quantity of adsorbent.

4. Conclusions

It has been demonstrated that MSP adsorbents synthesized via EISA method with optimal Surf/Si molar ratios of 0.12–0.18 have the characteristics of high surface area, narrow pore size distribution, and well-ordered hexagonal mesoporous structure. The surface area is proportional to the Surf/Si molar ratio up to 0.22. But the wall thickness between pores becomes thinner. The highest acetone adsorption capacity appears at S18 sample, which has a less specific surface area but a better pore structure as compared to the S22 sample. The better uniformity in the pore structure of S18 sample increases the rate of pore diffusion of acetone vapors and results in higher adsorption capacity as well as thinner mass transfer zone. The adsorption capacity of MSP made by EISA method is also superior to that of ZSM-5 zeolite used commercially by semiconductor and opto-electronic industries for abating VOCs emissions. In conclusion, the high adsorption capacity of S18 MSP reveals high potential to be a novel organic adsorbent.

Acknowledgments

The authors gratefully acknowledge financial supports of this work from the National Science Council of Taiwan under Contract nos. NSC 94-2211-E-009-046 and NSC95-2221-E-009-192. The helpful discussion with Dr. M. Karthik of the Institute of Environmental Engineering, NCTU, is also gratefully acknowledged.

References

Baccile, N., Grosso, D., Sanchez, C., 2003. Aerosol generated mesoporous silica particles. Journal of Materials Chemistry 13, 3011–3016.

Beck, J.S., Vartuli, J.C., Roth, W.J., Leonowicz, M.E., Kresge, C.T., Schmitt, K.D., Chu, C.T.W., Olson, D.H., Sheppard, E.W., Mccullen, S.B., Higgins, J.B., Schlenker, J.L., 1992. A new family of mesoporous molecular sieves prepared with liquid crystal templates. Journal of American Chemical Society 114, 10834–10843.

Bore, M.T., Rathod, S.B., Ward, T.L., Datye, A.K., 2003. Hexagonal mesostructure in powders produced by evaporation-induced self-assembly of aerosols from aqueous tetraethoxysilane solutions. Langmuir 19, 256–264.

Chang, F.T., Lin, Y.C., Bai, H.L., Pei, B.S., 2003. Adsorption and desorption characteristics of semiconductor volatile organic compounds on the thermal swing honeycomb zeolite concentrator. Journal of Air and Waste Management Association 53, 1384–1390.

Freundlich, H.M.F., 1906. Über die adsorption in lösungen. Zeitschrift für Physikalische Chemie 57, 385–471.

Kruk, M., Jaroniec, M., Sayari, A., 1997. Application of large pore MCM-41 molecular sieves to improve pore size analysis using nitrogen adsorption measurements. Langmuir 13, 6267–6273.

Langmuir, I., 1916. The constitution and fundamental properties of solids and liquids. Journal of American Chemical Society 38, 2221–2295.

Langmuir, I., 1918. The adsorption of gases on plane surfaces of glass, mica and platinum. Journal of American Chemical Society 40, 1361–1403.

Li, W., Zhang, M., Zhang, J., Han, Y., 2006. Self-assembly of cetyl trimethylammonium bromide in ethanol–water mixtures. Frontiers of Chemistry in China 4, 438–442.

Lin, Y.C., Bai, H., 2006. Temperature effect on pore structure of nanostructured zeolite particles synthesized by aerosol spray method. Aerosol and Air Quality Research 6, 42–53.

Lin, Y.C., Bai, H., Chang, C.L., 2005. Applying hexagonal nanostructured zeolite particles for acetone removal. Journal of Air and Waste Management Association 55, 834–840.

Lu, Y., Fan, H., Stump, A., Ward, T.L., Rieker, T., Brinker, C.J., 1999. Aerosol-assisted self-assembly of mesostructured spherical nanoparticles. Nature 398, 223–226.

Ruhl, M.L., 1993. Recover VOCs via adsorption on activated carbon. Chemical Engineering Progress 89 (7), 37–41.

Serrano, D.P., Calleja, G., Botas, J.A., Gutierrez, F.J., 2007. Characterization of adsorptive and hydrophobic properties of silicalite-1, ZSM-5, TS-1 and beta zeolites by TPD techniques. Separation and Purification Technology 54, 1–9.

Zhao, X.S., Lu, G.Q., Hu, X., 2001. Organophilicity of MCM-41 adsorbents studied by adsorption and temperature-programmed desorption. Colloids and Surfaces A: Physicochemical and Engineering Aspects 2001 (179), 261–269.